Nanoscale

Accepted Manuscript

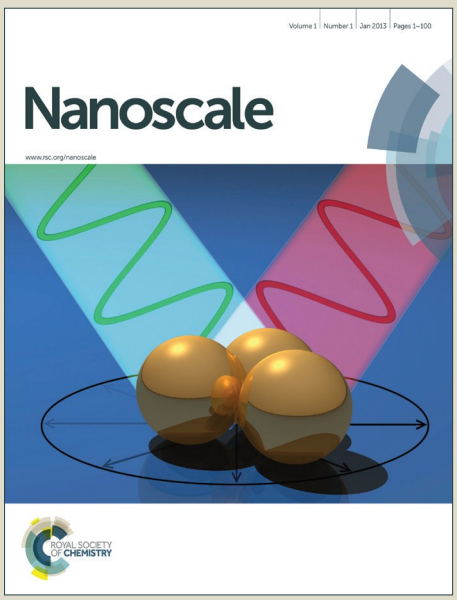

ROYAL SOCIETY OF CHEMISTRY

www.rsc.org/nanoscale

Carbon doped molybdenum disulfide nanosheets stabilized on graphene for hydrogen evolution reaction with high electrocatalytic ability

Yong Li, Jiao Wang, Xike Tian*, Longlong Ma, Chu Dai, Chao Yang, Zhaoxin Zhou

Faculty of Materials Science and Chemistry, China University of Geosciences, Wuhan 430074, PR China

*Corresponding author. Email address: xktian@cug.edu.cn; Tel.: +86 027 67883739

Abstract: Cost effective hydrogen evolution reaction catalyst without using precious metallic elements is a crucial demand for environment-benign energy production. In this work, the thin and rich-edge molybdenum disulfide nanosheets with carbon doped in the interlayers decorated on graphene were developed by a facile solvothermal process. The as-synthesized nanohybrids exhibited high catalytic ability over the hydrogen evolution electrochemical reaction with the onset overpotential of 0.165 mV and Tafel slope of 46 mV/dec. Furthermore, the prepared nanohybrids also showed the better durability and stability. Our work may build a potential method for *in situ* production of metal carbide–sulphur hybrid nanomaterials with promising applications for hydrogen evolution reaction.

Keywords: Molybdenum disulfide; Carbon doped; Graphene support; Hydrogen evolution reaction

1. Introduction

As a new class of material, transition metal dichalcogenides (TMDCs) have attracted enormous interest due to their excellent and unique optical, mechanical and electronic properties[1-5]. TMDCs are comprised of transition metal atoms which were surrounded in a sandwich structure by chalcogen atoms, and the chalcogen atoms between the layers were interacted with each other by the weak Vander Waals forces. TMDCs have an indirect band gap of 1.2 eV in the bulk, but their single layer has the direct energy gap of 1.8eV which is complementary to the zero-band gap graphene. Among the TMDCs, molybdenum disulfide (MoS_2), a kind of well-known TMDCs, has been widely applied as the lubricant and catalyst for hydrodesulphurization and hydrogen

evolutions[6]. Especially when MoS_2 as the catalyst for hydrogen evolution, density functional theory calculations have confirmed that the hydrogen binding energy of MoS_2 is close to Pt in the volcano curve[7], which makes MoS_2 a potentially low cost and abundance take place of Pt in hydrogen evolution reaction (HER). In addition, previous literatures have reported that the catalytic active sites of MoS_2 were mostly located along the edges of MoS_2 layers, while the basal planes are inert[8-10]. The MoS_2 nanosheets are catalytically active with many active unsaturated sulfur atoms; however the relatively low solubility and poor electrochemical durability greatly limited their practical application in HER[11-15]. So there is an urgent need to increase the amount of active sites, the activity of catalytic sites and the electrical communications between the active sites and the catalyst substrates of MoS_2 nanosheets. Xie's group has put forward the defect-rich MoS_2 ultrathin nanosheets and highlighted that the MoS_2 materials contained abundant defects, which arise from partial cracking of the catalytically inert basal planes, causing the exposure of additional active edge sites[16, 17]. Furthermore, the bulk 2H-MoS_2 crystal can be exfoliated by intercalation effect to transform into 1T-MoS_2, which has exhibited the dramatically enhanced HER catalytic ability[18,19]. In addition, the heteroatom doping may also modulate the electronic structure and frontier orbital energy of MoS_2 nanosheets to enhance the electrocatalytic abiltiy[20]. Developing an efficient strategy to realize heteroatom chemical doping and explore the dopant-related performance change of MoS_2 nanosheets still remain key challenges. Carbon is a kind of relatively un-reactive element, and has a potential voltage range of almost ideal polarizability, which is uniquely suitable for the construction of nanocatalysts with high electrochemical catalytic ability[21, 22]. Inspired by this, the combining of ultrathin MoS2 nanosheets and carbon element would enhance the interlayer spacing to increase the defects so as to develop the more efficient electrochemical nanocatalysts to improve the HER activity.

Although great advances have been achieved, the low conductivity of MoS_2 nanosheets would also greatly limit their applications. In addition, the aggregation of MoS_2 also affects the dispersion and results in the decrease of activity. Thus, it is important to design and develop an effective way that used conductive templates or supports to modify MoS_2 material to improve their catalytic activities. Graphene is such a kind of nanosheets which possess the high conductivity, large surface area, flexibility and chemical stability, and they can be used as the excellent substrates to host active nanomaterials for energy applications. In recent years, the

decoration of nanoparticles on graphene nanosheets has been widely investigated. Li's group proposed a selective solvothermal synthesis of MoS_2 nanoparticles on reduced graphene oxide sheets, which showed the high HER electrocatalytic activity[23]. A novel composite based on MoS_2 supported on WC decorated reduced graphene oxide was prepared through solvothermal method, where WC acted as a conductive dispersant to prevent graphene nanosheets from restacking, and the resulting catalyst exhibited excellent catalytic activity[24, 25].

Herein, the thin platelike and edge-rich MoS_2 nanosheets with carbon doped in the interlayers (C/MoS_2) were obtained by a one-step facile solvothermal method *via* just controlling the ratio of ethylene glycol and water. And then graphene nanosheets as support were introduced into C/MoS_2 nanohybrids (C/MoS_2@G) to improve the charge transfer of the material so as to enhance the electrocatalytic ability. The as-synthesized nanohybrids exhibited high catalytic ability over the hydrogen evolution electrochemical reaction with the onset overpotential of 0.165 mV and Tafel slope of 46 mV/dec. Furthermore, the prepared nanohybrids also showed the better durability and stability. Our work may build a potential method for *in situ* production of metal carbide –sulphur hybrid materials with promising applications for hydrogen evolution reaction.

2. Experimental

2.1 Materials and characterization techniques

Nafion solution (25%) was purchased from Sigma-Aldrich. Other chemicals used in the experiments were purchased from Sinopharm Chemical Reagent Co., Ltd of China. All of the reagents used herein were of analytical grade and used as received without any further purification. Water used in the experiments was deionized (DI) and doubly distilled prior to use.

The phase purity of the as-synthesized samples were analyzed by powder X-ray diffraction (XRD) with monochromatized Cu Kα (λ = 1.5406 Å) incident radiation by a Bruker AXS D8-Focus diffractometer operated at 40 kV voltage and 40 mA current with a scanning step of 0.05 second. Samples for TEM analysis were prepared by depositing a single drop of diluted NP dispersion on amorphous carbon coated copper grids. Transmission electron microscopy (TEM) images were acquired on a Philips CM 12 (120 kV) transmission electron microscope. High-resolution TEM (HRTEM) images were performed on a JEOL JEM-ARF2010FEF TEM/STEM with a spherical aberration corrector. Field emission scanning electron microscopy (FE-SEM) images were taken on a Hitachi SU-8010 scanning electron microscope operated at 30

kV equipped with an attached Oxford Link ISIS energy-dispersive X-ray spectroscopy (EDS). X-ray photoelectron spectroscopy (XPS) is obtained with a MULTILAB2000 electron spectrometer from VG Scientific using 300W Al Kα radiation. The Brunauer–Emmett–Teller (BET) specific surface area of the sample was analyzed by nitrogen adsorption in a Micromeritics ASAP 2020 nitrogen adsorption apparatus. All samples were dried before characterization by an oven to remove the adsorbed water.

2.2 Synthesis of MoS_2 and C/MoS_2 nanosheets

The MoS_2 and C/MoS_2 nanosheets were prepared by a facile solvothermal method. 0.5 mmol of $(NH_4)_6Mo_7O_{24}\cdot 4H_2O$ and 10 mmol of thiourea were dissolved in a 40 mL mixture solution of ethylene glycol and water with the volume ratio of 1:1 and 0:1. The mixture solution was stirred for 2 h to form a homogeneous solution and then transferred to an 80 mL Teflon-lined autoclave, sealed and heated in an oven at 210℃ for 24 h. The products were cooled, collected and washed with massive water and ethanol for several times. Finally, the products were dried in a vacuum oven at 60℃ for 24h. When the solution is water only, the final product was denoted as MoS_2 nanosheets. When the solution is the mixture solution of glycol and water with the volume ratio of 1:1, the final product was denoted as C/MoS_2 nanosheets.

2.3 Synthesis of C/MoS_2@G nanosheets

Graphene oxide nanosheets with the concentration of 5.525 g/L were prepared according to the previous modified Hummers method [26]. 0.5 mmol of $(NH_4)_6Mo_7O_{24}\cdot 4H_2O$ and 10 mmol of thiourea were dissolved in a mixed solution of ethylene glycol and water with the volume ratio of 1:1. The mixture solution was stirred for 2 h to form a homogeneous solution. And then the appropriate amount of graphene oxide nanosheets was dropwise added to the above homogeneous solution. The solution was stirred for 4 h, and then transferred to a vessel to sonicate for 1 h. Finally, The mixture solution was transferred to a Teflon-lined autoclave, sealed and heated in an oven at 210 ℃ for 24 h. The hydrogel product, C doped MoS_2 nanosheets decorated on graphene (C/MoS_2@G), was collected and washed with massive water and ethanol for several times, and dried in a frozen oven for 48 h. According to different amount of graphene oxide in the preparation process, the mass fractions of graphene support in the final samples are 2%, 4%, 8% and 10%, and these final samples C/MoS_2@G can be denoted as C/MoS_2@G_1, C/MoS_2@G_2, C/MoS_2@G_3 and C/MoS_2@G_4, respectively.

2.4 Electrochemical measurements

All of the electrochemical measurements for the samples were performed using a glassy carbon electrode in a three-electrode system on an electrochemical workstation (CHI660C). 4 mg of catalyst and 20 μL of Nafion solution were dispersed in 1 mL water-ethanol mixture solution, and the solution was sonicated for 40 min to form a homogeneous ink. Then 5 μL of the dispersion was loaded onto a glassy carbon electrode with 3 mm diameter. The electrochemical measurements were performed in 0.5mol/L H_2SO_4 electrolyte solution using Ag/AgCl (saturated KCl) and a graphite rod as the reference electrode and the counter electrode, respectively. The potential were calibrated to the reversible hydrogen electrode (RHE). Line sweep voltammetry were taken with a 5 mV/s scan rate. The Nyquist plots were performed with frequencies ranging from 100 kHz to 0.01Hz at an overpotential of 300 mV.

3. Results and discussion

The C/MoS_2@G nanohybrids were prepared by the decoration of C/MoS_2 nanosheets onto graphene surface. And the C/MoS_2 ultrathin nanosheets were simply prepared by a facile solvothermal method controlling the volume ratio of ethylene glycol and distilled water. The change of the amount of ethylene glycol would lead to the different states of carbon incorporation. And the disorder engineering during this process would lead to the formation of carbon doped MoS_2 nanosheets.

The crystal structures of MoS_2, C/MoS_2 and C/MoS_2@G nanosheets were investigated by XRD measurements. As shown in Fig. 1a, the MoS_2 ultrathin nanosheets can be obtained when the reaction solvent is water only, and their diffraction peaks were well matched with the hexagonal phase of MoS_2 (2H-MoS_2, JCPDS Card No.75-1539). And the low intensity of the (002) diffraction peak suggests the low crystallinity. However, when the volume ratio of ethylene glycol and water is 1:1, C/MoS_2 nanosheets can be obtained. And their (002) diffraction peak disappeared with two new peaks emerging at the low-angle regions. In addition, the intensity of (004), (100), (102), (110) diffraction peaks also decreased, which suggested that the crystallinity decreased a lot compared to the 2H-MoS_2 ultrathin nanosheets. Detailed analysis of these two peaks showed that the corresponding d spacings were 9.50 Å and 4.8 Å, respectively, showing that the new structure was formed. Especially, the structure enlarge interlayer spacing of 9.50 Å compared with that of 6.5Å of 2H-MoS_2,

indicating that C/MoS_2 nanosheets were successfully prepared. To further analyze the structure information of C/MoS_2 ultrathin nanosheets, C/MoS_2 ultrathin nanosheets were annealed. In Fig. 1b, we found that XRD pattern of C/MoS_2 nanosheets changed. Two new peaks emerged at the low-angle region which replaced the (002) characteristic peak of 2H-MoS_2. Thus, the new structure with MoS_2 layers is identified and has the weak stability and conductivity. In the order to improve the electrocatalytic ability, C/MoS_2@G nanohybrids were prepared. For the XRD patterns of C/MoS_2@G nanohybrids (Fig. 1a and Fig. S1), we can easily notice that the peak marked by the arrow corresponds to the diffraction peak of graphene, indicating that graphene nanosheets were integrated onto C/MoS_2 nanosheets to produce the C/MoS_2@G nanohybrids.

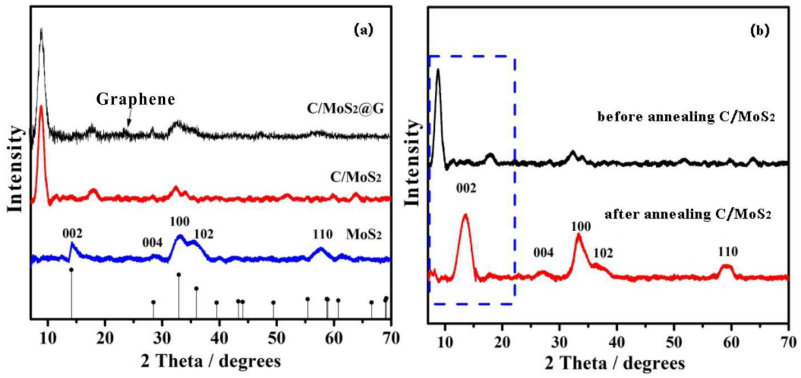

Fig. 1 (a) XRD patterns of MoS_2, C/MoS_2 and C/MoS_2@G; (b) XRD pattern of C/MoS_2 nanosheets before and after annealing.

The morphologies of C/MoS_2 nanosheets and C/MoS_2@G nanohybrids were characterized by FESEM and TEM. FESEM images of C/MoS_2 nanosheets and C/MoS_2@G nanohybrids were shown in Fig. 2a and 2b. As shown, the FESEM image of C/MoS_2 nanosheets clearly shows the thin platelike nanosheets morphology, and the lateral size of the nanosheets is in the range of 100-180 nm. While the FESEM images of C/MoS_2@G nanohybrids (Fig. 2b and Fig. S2) showed that the C/MoS_2@G nanohybrids are a kind of plate-like structure, which is helpful to increase the specific area of the nanohybrids. In the nanohybrids, the overlapping or coalescing of the graphene will form an interconnected conducting network, and facilitate rapid electronic transport in electrode reactions. In addition, this plate-like structure also can enhance the stability of the nanohybrids due to the super strength of graphene. The

representative TEM image (Fig. 2c) of C/MoS_2 nanosheets also indicates their thin platelike nanosheet morphology. While the typical TEM images of the synthesized C/MoS_2@G nanohybrids (Fig. 2d and Fig. S3) reveals that the thin and plate-like C/MoS_2 nanosheets were homogeneously embedded in the graphene nanosheets, as marked by the arrow.

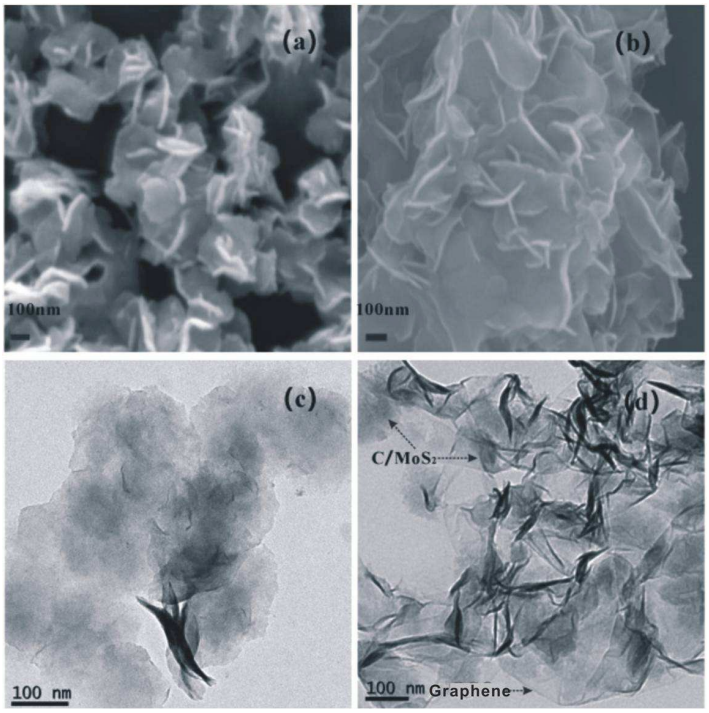

Fig. 2 FESEM images of C/MoS_2 nanosheets (a) and C/MoS_2@G nanohybrids (b); TEM images of C/MoS_2 nanosheets (c) and C/MoS_2@G nanohybrids (d).

The structure of C/MoS_2@G nanohybrids was further confirmed by HRTEM (Fig. 3). As shown in Fig. 3a, we can clearly see that a great number of MoS_2 crystal fringes (marked by red circle) were dispersed onto the amorphous graphene nanosheets (marked by yellow circle). The red region of the HRTEM image was also studied by FFT and inverse FFT (Fig. 3b). From the *inset* of Fig. 3b, the FFT pattern of C/MoS_2@G with six weak diffraction points indicated the weak crystallinity. Meanwhile, the inverse FFT pattern (Fig. 3b) exhibits rich defects in the structure, as marked by the red circle. In addition, the interplanar spacings of 2.7Å and 1.58 Å are corresponding to the d spacing of (100) and (111) planes. The side-view HRTEM image (Fig. 3c) shows the interlayer spacing of 9.8 Å, which is greater than that of the C/MoS_2 ultrathin

nanosheets. It may be due to that the appropriate amount of RGO enlarged the interlayer spacing. In addition, we can observe the rich defects from the HRTEM images of C/MoS_2@G nanohybrids, which can increase the electrocatalytic sites and the catalytic ability. In order to further verify the structure of C/MoS_2@G, we need to study the structure of C/MoS_2 nanosheets detailedly. As shown, the HRTEM image of C/MoS_2 nanosheets in top view (Fig. 3d) was obtained. We can observe the degree of disorder and many defects. In order to clearly estimate the extent of the disorder and the amount of the defects, the red region of the HRTEM image was studied by the fast Fourier transform (FFT) and inverse FFT, from which the individual between the rotational angles can be identified[27-30]. From the *inset* of Fig. 3e, the FFT pattern of C/MoS_2 possesses six weak diffraction points, suggesting the existence of the slight disorders. Meanwhile, the inverse FFT pattern (Fig. 3e) exhibits rich defects in the structure. We can obtain the interplanar spacing of 2.7Å, which is corresponding to the d spacing of (100) planes. And the spacing of 1.58 Å is the d spacing of (110) planes. The rich defects were marked by the red circles, which can be attributed to the C doped and the quasi periodic structure. In addition, the side-view HRTEM image (Fig. 3f) shows the interlayer spacing of 9.6 Å, which is greater than the normal 2-H MoS_2 nanosheets, and the experimental result is consistent with the result of XRD[31]. As shown in Fig. 3f, the curled edge exhibits C/MoS_2 nanosheets are consisted of 4-8 layers. There is an interesting observation that the crystal fringes along the curled edge are discontinuous, which increased the defects and increased the electrocatalytic sites.

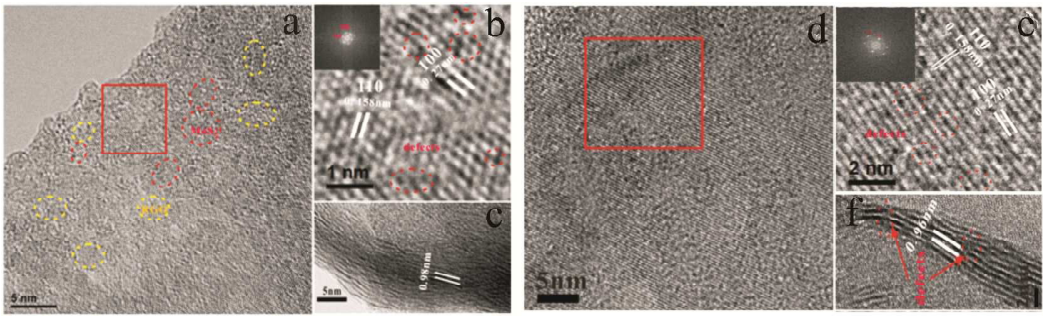

Fig. 3 HRTEM image in top view (a), FFT and the inverse FFT of the red region (b) and HRTEM image in side view of C/MoS_2@G nanohybrids (c); HRTEM image in top view (d), FFT and the inverse FFT of the red region (e) and HRTEM image in side view of C/MoS_2 nanosheets (f).

In order to investigate the chemical states of Mo and S in the plate-like C/MoS2@G nanohybrids, XPS spectra were carried out. As shown in Fig. 4a, the characteristic peaks at 228.9 and 233.1 eV are attributed to Mo $3d_{5/2}$ and Mo $3d_{3/2}$ binding energies for a Mo (IV) oxidation state. The S 2p region of C/MoS_2@G nanohybrids (Fig. 4b) exhibits the $2p_{3/2}$ and $2p_{1/2}$ peaks at the 161.6 and 162.7 eV, which is consistent with divalent sulfide ion (S^{2-}). The peaks for S 2p at 163.4 and 164.1 eV indicated the presence of bridging S^{2-} or S_2^{2-}, which was resulted from the unsaturated S atoms. For the C 1s spectra, the peak located at 286.2 eV can be attributed to the adventitious carbonic oxide. The peaks at 284.7, 285.5 and 286.6 eV of C 1s spectra (Fig. 4c) indicate the existence of C-C, C-O and C=O. Thus, the experimental results provided evidences that graphene oxide nanosheets were reduced to graphene. In addition, the existence of Mo-C was also confirmed by the peak at 283.6 eV in the C 1s spectra. Generally, carbon atoms were successfully doped in the MoS_2 nanosheets, and C/MoS_2 nanosheets were well dispersed onto the graphene surface. The N_2 adsorption–desorption isotherms for C/MoS_2@G with the graphene of 4% have also been conducted. As shown in Fig. 4d, C/MoS_2@G nanohybrids have representative type-IV curves in adsorption and desorption isotherms at a relative pressure range of 0–1.0, which can be attributed to capillary condensation and multilayer adsorption/desorption of nitrogen in the mesopores or macropores. In addition, the C/MoS_2@G nanohybrids exhibited a relative high BET specific surface area of 65.56 m^2/g, which is greater than that of MoS_2 nanosheets of 2.64 m^2/g[31]. That may be due to the doping of carbon and the support of graphene, which is beneficial to the improvement of electrocatalytic ability.

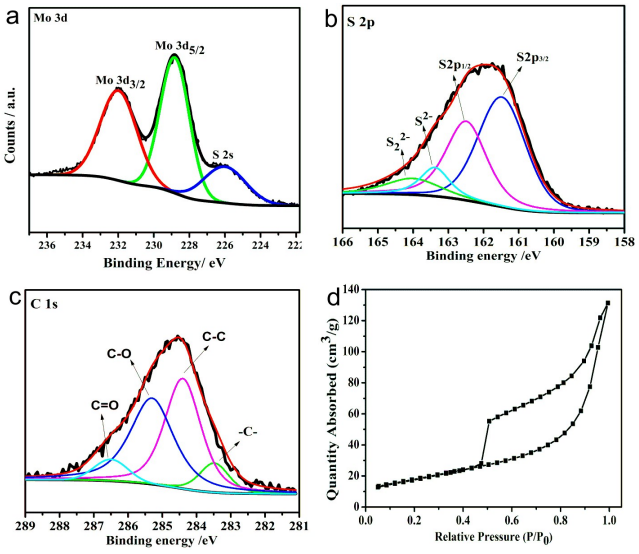

Fig. 4 XPS survey scans of Mo 3d (a), S 2p (b), C 1s (c) spectra, and N_2 adsorption–desorption isotherms (d) of C/MoS_2@G nanohybrids.

Firstly, we studied the electrocatalytic HER activities of C/MoS_2@G nanohybrids with different amount of graphene (C/MoS_2@G_1, C/MoS_2@G_2, C/MoS_2@G_3, and C/MoS_2@G_4) which were deposited on a glassy carbon electrode in 0.5 M H_2SO_4 solution using a typical three electrode setup. As shown in Fig. S4, linear sweep voltammetry (LSV) of the C/MoS_2@G nanohybrids were carried out. Obviously, we can find that the current density of C/MoS_2@G_2 with 4% graphene is higher than that of other nanohybrids when the onset overpotential is -0.35 V (*vs* RHE), showing that C/MoS_2@G_2 is the best electrocatalyst among these nanohybrids. The graphene support plays an important role in HER, which increases the transferring rate of the charge, thus enhancing the electrocatalytic ability. In addition, the appropriate amount of graphene is also important. When the mass fraction of graphene is 4%, the electrocatalytic ability is highest. While increasing the graphene amount, the electrocatalytic decreases. That may be due to that the active sites only exist on the MoS_2 nanosheets, while no active sites exist on the graphene nanosheets. Increasing the graphene amount would decrease the active sites of MoS_2 nanosheets, thus decreasing the electrocatalytic ability. Furthermore, the electrocatalytic HER activities of the MoS_2, C/MoS_2 and C/MoS_2@G_2 deposited on a glassy carbon electrode in 0.5 M H_2SO_4 solution were investigated. We also performed measurements using a commercial Pt catalyst which exhibits high HER catalytic activity with nearly zero onset overpotential, as the contrast experiment. As shown in Fig. 5a, LSV of C/MoS_2 and C/MoS_2@G_2 ultrathin nanosheets were carried out. They possess the much lower onset overpotentials of 0.25 and 0.165V, respectively, than the MoS_2 catalysts. The C doped MoS_2 nanosheets supported by graphene can improve the internal electrical conductivity and the rich S atoms that the bridging disulfides S_2^{2-} and apical S^{2-} are present in the structure to increase the active sites for HER. It has been confirmed that the C doping and the graphene support can greatly enhance the electron-donor or basic capacities of the material, improving the HER activity.

Moreover, the corresponding Tafel plots of MoS_2, C/MoS_2, C/MoS_2@G_2 and Pt are shown in Fig. 5b. Their Tafel slopes are 93 mV/dec, 60 mV/dec, 46 mV/dec and 30 mV/dec, respectively. The HER is the a half reaction of water splitting, which has three principle steps for converting H^+

to H_2 in the acidic medium[32, 33]. The first is named as the Volmer reaction (Equation 1) which is an initial discharge step, and the other are Heyrovsky (Equation 2) and Tafel reactions (Equation 3) which are the electrochemical desorption step and recombination step.

$$H_3O^+ + e^- \rightarrow H_{ads} + H_2O \quad (1)$$

$$H_{ads} + H_3O^+ + e^- \rightarrow H_2 + H_2O \quad (2)$$

$$H_{ads} + H_{ads} \rightarrow H_2 \quad (3)$$

Tafel slope is an important inherent property of electrocatalysts that is determined by the rate-limiting step of HER according to the published literatures[34, 35]. When the Volmer reaction is the rate-controlling step of HER, we can obtain a slope of 120 mV/dec in the specific set of conditions. While Tafel slopes of 30 and 40 mV/dec should be observed if the Heyrovsky or Tafel reactions act as the rate-controlling step, respectively. For a complete HER process, Volmer–Heyrovsky mechanism or Volmer–Tafel mechanism is combined which should be referred to produce H_2 molecules. For the Tafel slope of MoS_2 (93 mV/dec) and C/MoS_2 nanosheets (60 mV/dec), it is evident that the electrocatalytic ability was enhanced due to that carbon was doped into the interlayers of MoS_2 nanosheets to increase the interlayer spacing. In addition, we can find the Tafel slope decreased greatly when C/MoS_2 nanosheets were decorated on graphene to obtain C/MoS_2@G nanohybrid, which is due to that the overlapping or coalescing of the graphene will form an interconnected conducting network, and facilitate rapid electronic fast transport in electrode reactions. In addition, this plate-like structure also can enhance the stability of the nanohybrids due to the super strength of graphene so as to decrease the Tafel slope to enhance the electrocatalytic ability toward HER. In order to prove the interface reactions and intrinsic conductivity for the samples, the electrochemical impedance spectroscopy (EIS) is carried out to investigate the kinetics of the catalysts under HER process. As shown in Fig. 5c, we can see the semicircle in the Nyguist plots which reveal a significantly decreased charge-transfer resistance (R_{ct}) for MoS_2 (205.7 Ω), C/MoS_2 (72.2 Ω), and C/MoS_2@G_2 (13.2 Ω). The EIS results suggest that the C doping and graphene supported indeed optimized the electrical properties improving the intrinsic conductivity and the graphene as the conductive substrates which enhance the interdomain conductivity to faster transfer the charge.

Finally, durability is anther desired criterion to evaluate an advanced electrocatalyst. In order to investigate the durability of C/MoS_2@G_2 nanosheets, the C/MoS_2@G_2 electrocatalyst has been

cycled continuously for 1000 cycles. As shown in Fig. 5d, the negligible decay can be observed that indicates the excellent stability of C/MoS_2@G_2 electrocatalyst in a long-term electrochemical process. In general, the C/MoS_2@G nanohybrids have the excellent catalyst activity and high stability over HER.

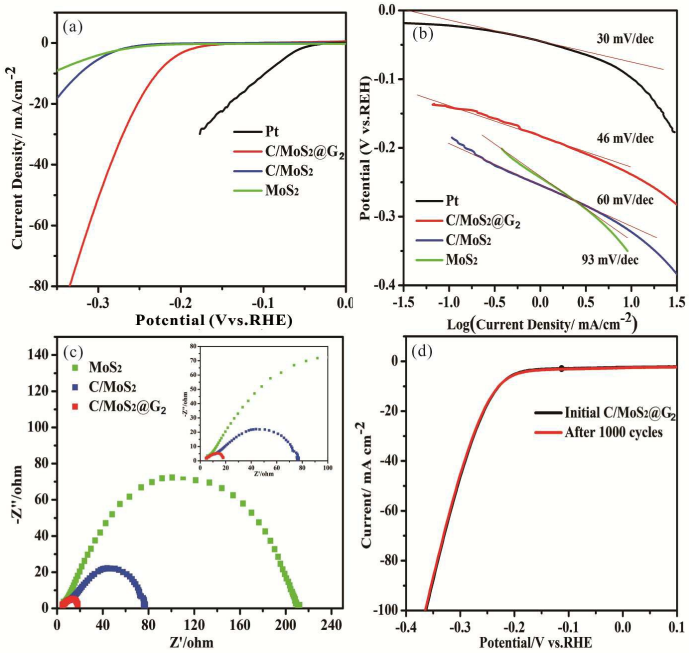

Fig. 5 (a) Polarization curves and (b) corresponding Tafel plots of MoS_2, C/MoS_2, C/MoS_2@G_2 and Pt, (c) Nyquist plots of MoS_2, C/MoS_2, C/MoS_2@G_2 nanosheets, (d) Polariztion curves revealing that negligible degradation of HER activity is observed for C/MoS_2@G_2 nanohybrids after 1000 cycles.

4. Conclusions

In conclusion, we have successfully synthesized and characterized the C/MoS_2@G ultrathin nanohybrids by a facile method. For the nanomaterials, the plate-like and edge-rich nanohybrids with carbon doped in the interlayers not only enlarge the distance between the layers, but also increase the defects in the basic plane, exhibiting better catalyst activity than the MoS_2 nanosheets. In addition, the C/MoS_2 nanosheets were supported onto graphene, and the graphene nanosheets were acted as a channel for transferring electrons and enhance the interactions between increasing the active edges and the whole MoS_2 nanosheets. Mass fractions of graphene support in C/MoS_2@G nanohybrids with 4% is the best electrocatalyst among these nanohybrids, which

exhibited an much higher HER electrocatalytic ability than C/MoS_2 nanosheets with the onset potentials of -0.16 V (vs RHE) and a low Tafel slope of 46 mV/dec. The mechanism of HER is according to the Volmer–Heyrovsky mechanism. In addition, the C/MoS_2@G nanohybrids can be cycled continuously for 1000 cycles without any electrocatalytic ability loss, exhibiting high durability. This study successfully indicates that carbon doped and graphene supported edge-rich and thin nanosheets MoS_2 is feasible by a facile solvent-dependent control method and exhibited high electrocatalytic ability for HER.

Acknowledgements

This work was supported by the National Basic Research Program of China (Grant No. 2011CB933700), the National Natural Science Foundation of China (Grant NO. 51371162) and the Fundamental Research Funds for the Central Universities, China University of Geosciences (Wuhan) (No.2014029).

Notes and references

1 K. J. Huang, L. Wang, Y. J. Liu, H. B. Wang, Y. M. Liu and L. L. Wang, *Electrochim. Acta*, 2013, **109**, 587.

2 G. Eda, H. Yamaguchi, D. Voiry, T. Fujita, M. W. Chen and M. Chhowalla, *Nano Lett.*, 2011, **11**, 5111.

3 A. Splendiani, L. Sun, Y. B. Zhang, T. S. Li, J. Kim, C. Y. Chim, G. Galli and F. Wang, *Nano Lett.*, 2010, **10**, 1271.

4 Z. Y. Yin, H. Li, H. Li, L. Jiang, Y. M. Shi, Y. H. Sun, G. Lu, Q. Zhang, X. D. Chen and H. Zhang, *ACS Nano*, 2012, **6**, 74.

5 S. Bertolazzi, J. Brivio and A. Kis, *ACS Nano*, 2011, **5**, 9703.

6 E. Furimsky, *Catal. Rev.*, 1980, **22**, 371.

7 S. Trasatti, *J. Electroanal. Chem. Interfacial Electrochem.*, 1971, **33**, 351.

8 W. Jaegermann and H. Tributsch, *Prog. Surf. Sci.*, 1988, ***29*** , 1 .

9 B. Hinnemann, P. G. Moses, J. Bonde, K. P. Jørgensen, J. H. Nielsen, S. Horch, I. Chorkendorff and J. K. Nørskov, *J. Am. Chem. Soc.*, 2005, **127**, 5308.

10 T. F. Jaramillo, K. P. Jørgensen, J. Bonde, J. H. Nielsen, S. Horch and I. Chorkendorff, *Science*,

2007, **317**, 100.

11 D. Merki and X. Hu , *Energy Environ. Sci.*, 2011, **4**, 3878.

12 J. D. Benck , Z. Chen, L. Y. Kuritzky, A. J. Forman and T. F. Jaramillo, *ACS Catal.*, 2012, **2**, 1916.

13 A. B. Laursen, P. C. K. Vesborg and I. Chorkendorff, *Chem. Commun.*, 2013, **49**, 4965.

14 Y. H. Chang, C. T. Lin, T. Y. Chen, C. L. Hsu, Y. H. Lee, W. Zhang, K. H. Wei and L. J. Li, *Adv. Mater.*, 2013, **25**, 756.

15 D. Merki, S. Fierro, H. Vrubel and X. Hu, *Chem. Sci.*, 2011, **2**, 1262.

16 J. Xie, H. Zhang, S. Li, R. Wang, X. Sun, M. Zhou, J. Zhou, X. W. Lou and Y. Xie, *Adv. Mater.*, 2013, **25**, 5807.

17 J. Xie, J. Zhang, S. Li, F. Grote, X. Zhang, H. Zhang, R. Wang, Y. Lei, B. Pan and Y. Xie, *J. Am. Chem. Soc.*, 2013, **136**, 1680.

18 S. S. Jiménez, D. Yang, R. F. Frindt and J. C. Irwin, *Phys. Rev. B*, 1991, **44**, 3955.

19 F. Wypych and R. Schollhorn, *Chem. Commun.*, 1992, 1386.

20 X.Q. Lin and J.Ni, *J. Appl. Phys.*, 2014, **116**, 044311.

21 Y.N. Yan, T. Kuila, N.H. Kim, B.C. Ku and J.H. Lee, *J. Mater. Chem. A*, 2013, **1**, 5892.

22 H. Kim, M.E. Fortunato, H. Xu, J.H. Bang and K.S. Suslick, *J. Phys. Chem. C*, 2011, **115**, 20481.

23 Y. Li, H. Wang, L. Xie, Y. Liang, G. Hong and H. Dai, *J. Am. Chem. Soc.*, 2011, **133**, 7296.

24 Y. Yan, B. Xia, X. Qi, H. Wang, R. Xu, J. Y. Wang, H. Zhang and X. Wang, *Chem. Commun.*, 2013, **49**, 4884.

25 L. H. Bennett, J. R. Cuthill, A. J. McAlister, N. E. Erickson and R. E. Watson, *Science*, 1974, **184**, 563.

26 H. Wang, L. F. Cui, Y. Yang, H. S. Casalongue, J. T. Robinson, Y. Liang, Y. Cui and H. Dai, *J. Am. Chem. Soc.*, 2010, **132**, 13978.

27 K. Kim, Z. Lee, W. Regan, C. Kisielowski, M. F. Crommie and A. Zettl, *ACS Nano*, 2011, **5**, 2142.

28 P. Y. Huang, C. S. Ruiz-Vargas, A. M. van der Zande, W. S. Whitney, M. P. Levendorf, J. W. Kevek, S. Garg, J. S. Alden, C. J. Hustedt, Y. Zhu, J. Park, P. L. McEuen and D. A. Muller, *Nature*, 2011, **469**, 389.

29 A. L. Gibb, N. Alem, J. H. Chen, K. J. Erickson, J. Ciston, A. Gautam, M. Linck and A. Zettl, *J. Am. Chem. Soc.*, 2013, **135**, 6758.

30 J. An, E. Voelkl, J. W. Suk, X. Li, C. W. Magnuson, L. Fu, P. Tiemeijer, M. Bischoff, B. Freitag, E. Popova and R. S. Ruoff, *ACS Nano*, 2011, **5**, 2433.

31 W. Qin, T. Chen, L. Pan, L. Niu, B. Hu, D. Li, J. Li and Zhuo Sun, *Electrochim. Acta*, 2015, **153**, 55.

32 Y. Sun, X. Hu, W. Luo and Y. Huang, *ACS Nano*, 2011, **5**, 7100.

33 N. Pentland, J. O. M. Bockris and E. J. Sheldon, *Electrochem. Soc.*, 1957, **104**, 182.

34 J. O'M. Bockris, in: J. O'M. Bockris, B.E. Conway (Eds.), Chapter 4 in Modern Aspects of Electrochemistry, vol. 1, Butterworths Sci. Publications, London, 1954.

35 B. E. Conway, B. V. Tilak, in: D.D. Eley, H. Pines, P.B. Weisz (Eds.), Chapter 1 in Advance in Catalysis, vol. 38, Academic Press Inc., New York, 1992.